Data visualization for reliability analysis of repairable systems

Gámiz, M.L.[1], López-Montoya, A.J., Martínez-Miranda, M.D., Raya-Miranda, R.

University of Granada (Spain)

Abstract

The objective of this paper is to find out possible patterns of failure occurrences in a repairable system. We develop a graphical exploratory tool and perform visual inference considering nonparametric local linear kernel estimators for the rate of occurrence of failures (ROCOF) and its first derivative. The shape characteristics of the ROCOF function are distinguished from those which are merely an artifact of the sampling variability of the data through the construction of confidence intervals for the first derivative. The proposal is illustrated with several real datasets, and its performance is evaluated through an extensive simulation study.

Keywords: ROCOF; NHPP rate; SiZer; Kernel smoothing; Bootstrap.
2010 MSC: 62-07, 62-09

Nomenclature

ROCOF	Rate of occurrence of failures
NHPP	Nonhomogeneous Poisson process
SiZer	Significant zero crossing of derivatives
ESS	Effective sample size
$A^\top$	Transpose of a matrix A
$\arg\min_\theta S(\theta)$	Value of θ for which $S(\theta)$ is minimum
$\widehat{\theta}$	An estimator of θ
Φ^{-1}	Inverse cumulative distribution function of standard Normal
$\xrightarrow{P}$	Convergence in probability
$\xrightarrow{D}$	Convergence in distribution
$C_v([0,t])$	Space of functions with v continuous derivatives in $[0,t]$, $t>0$
$o_P(\cdot)$	$X_n = o_P(a_n) \Leftrightarrow a_n^{-1} X_n \xrightarrow{P} 0$, as $n \to +\infty$; for X_n random variable ($r.v.$), and $a_n \in \mathbb{R}$

Email address: mgamiz@ugr.es (Gámiz, M.L.)
[1]Corresponding author

1. INTRODUCTION

It is usually understood that a repairable system works as follows: it is put into operation, it fails, it is repaired, it is put back into satisfactory operational conditions and so on. When the time duration of times between failures varies, increasing or decreasing, it is obvious that the number of failures occurring within successive, equally spaced time intervals decreases or increases respectively. The quantity that describes failures per unit time was defined by Ascher and Feingold[1] as the rate of occurrence of failures (ROCOF). It gives the pattern of occurrences in a repairable system and it is computed in terms of the first derivative of the expected number of failures.

Traditionally, the literature on repairable systems is concerned with stochastic modelling based on point process theory. A typical reference is Ascher and Feingold[1] and an updated revision on the subject, including recent theoretical developments on point processes and applications on reliability analysis, is presented in Cha and Finkelstein[2]. The most commonly used models for the failure process of a repairable system are renewal processes (RP), and nonhomogeneous Poisson processes (NHPP). Lindqvist *et al.*[3] and Lindqvist[4] study some generalizations of these models. In particular they consider the Trend Renewal Process (TRP) that includes NHPP and RP as special cases.

The features of a point process are determined by its conditional intensity function. In this paper we consider counting processes that fit the multiplicative intensity model presented in Aalen[5], which assumes that the intensity function of the counting process can be decomposed into a product of a purely deterministic factor (hazard) and an observable stochastic factor. One simple particular case of this kind of processes is the NHPP that assumes that after each failure the system is returned to identical operational conditions it was just before the failure, i.e. *minimal repair* is being carried out by the system environment. This occurs frequently in a very natural way, in particular when a system is large. In such a case, upon failure of the system, repair (or perhaps replacement) of only a small part may change the state of the system from failed to working without affecting the system in any other sense. More general examples of counting processes fitting the Aalen multiplicative intensity model are the Cox proportional intensity process, where the heterogeneity of the population of systems can be accounted by the model, and the generalized Polya process, where the independent increments property that defines the NHPP is relaxed (see Cha and Finkelstein[2]).

For data analysis concerns, Aalen model is a quite general model which has shown to be acceptable for a large number of practical situations in many applied areas where the interest is in event history analysis, see Andersen *et al.*[6] for discussion of a large list of examples as well as for an exhaustive statistical analysis of counting processes under the Aalen model. The methods presented in this paper are developed for a class of counting processes that fit the model of Aalen. The real examples discussed in Section 5 are previously tested in order to decide whether this assumption is acceptable or not. To do it we consider a graphical procedure that has been adapted here from the nonparametric techniques presented in Gámiz and Lindqvist[30].

As pointed out in Krivtsov[7], an overwhelming majority of publications on NHPPs considers just two monotonic forms of the NHPP's ROCOF: the log-linear model and the power law model. In his paper, the author claims the fact that the NHPP intensity rate formally

coincides with the hazard function of the underlying lifetime distribution. Therefore, the variety of parametric forms for the hazard functions of traditional lifetime distributions could be used as the models for the ROCOF of respective NHPPs. In consequence he concludes that parameter estimation of such ROCOF models reduces to the estimation of the cumulative hazard function of the underlying lifetime distribution. For a recent discussion on the subject see Wang and Lu[8] and references therein.

In this aim, statistical modelling based on data analyses is a highly valuable tool that engineers can employ to optimize the performance of assets under their supervision. An inadequate parametric approach leads to erroneous model selection for the failure time of the system, which can in turn induce to wrong decisions for the system maintenance procedure thus involving serious economical problems, among others. In conclusion, statistical analyses based on false (parametric) premises about the system lifetime lead to erroneous model selection which, in the best of the cases, turn out to be useless for reliability analysts. On the one hand, in certain situations, a fully detailed description of the *time-system* relationship is not necessary. Rather, what the reliability analyst needs to know, to implement an efficient (preventive and/or corrective) maintenance policy for the system, is just appropriate and useful information about the critical trend changes of the ROCOF. The knowledge about the existence of peaks in the intensity function curve might help the analyst to anticipate the occurrence of failures and thus more efficiently programming a preventive maintenance policy. On the other hand, in case the analyst needs to explicitly construct a parametric model for the system lifetime (for forecasting purposes for example), a previous trend-changes analysis of the failure rate would be very useful for an adequate model selection. Although many well-known life distributions that show monotone failure rate and are typical models used as intensity models for counting failure processes, there exist several situations for which the monotonicity assumption does not model the tendency to failure properly. Therefore trend change of failure rate has been an important subject of study for engineers. See for example references[9,10,11,12], just to cite some recent studies.

Having in mind all the above considerations, the main purpose of this paper is to provide an effective graphical tool to explore the underlying characteristics of the ROCOF, in order to detect constant or monotonic patterns, or possible trend changes. Our practical motivation is the study presented in Phillips[13] where the author develops bootstrap methods for constructing confidence regions for the ROCOF of a repairable system, in particular he analyses the failure times of a photocopier. That paper shows up the advantages of kernel smoothing to detect local features of the ROCOF such as changes of trend. A rigid parametric approach such as the power-law estimate is not able to reveal such trend changes. Kernel estimators depend on smoothing (bandwidth) parameters which need to be chosen in practice. Moreover different choices of the bandwidth can lead to very different outcomes in some cases, which can be tricky to interpret (see Section 3). Phillips[13] deals with this problem choosing the bandwidth by cross-validation, and therefore the conclusions in the paper rely on a unique curve estimation. This approach has the problem that some features in the data can be only revealed looking at a wide range of bandwidth values. With this idea Chaudhuri and Marron[14] introduced the inferential graphical tool SiZer to detect significant local features in density and regression functions. SiZer (shortening of "significant zero crossing of the derivatives") utilizes kernel smoothing to estimate the underlying

structure in the data and plays with the smoothing parameter, as a scale parameter, to visualize the underlying characteristics in the target function. The characteristics that are really there, that is, those which are not an artefact of the sampling variability, are revealed through the construction of confidence intervals for the first derivative of the function. See Marron and de Uña Álvarez[15], Godtliebsen and Oigard[16], González-Manteiga *et al.*[17], Martínez-Miranda *et al.*[18], Park *et al.*[19,20], for recent appealing extensions.

This paper provides an extension of SiZer for the rate function of a counting process under the Aalen's multiplicative intensity model. The first step in developing SiZer is to define a proper kernel estimator for the ROCOF and its first derivative, as the characteristics of the function are identified by the sign of the first derivative. Section 2 describes local linear kernel estimators for the failure rate function and its first derivative, which arise from the intuitive least squares principle suggested by Nielsen and Tanggaard[21] for hazard estimation. By exploiting the properties of the assumed model for the arrival process it is possible to derive straightforward closed-form expressions for the variance of these estimators. Closely related local linear estimators have been proposed by Chen *et al.*[22] for counting process intensity functions, but considering martingale estimating equations. Section 3 illustrates the effect of the bandwidth on the estimated ROCOF considering the classic coal mining disaster data. The second step is to construct confidence intervals for the intensity rate derivative to allow the inference about the trend changes in the failure rate. Section 4 describes two alternative methods to construct confidence intervals, one based on the asymptotic Normal distribution and other based on a consistent bootstrap method suggested by Cowling *et al.*[23]. Both methods have been considered to define pointwise and simultaneous confidence intervals. Four applications to real data are described in Section 5. The empirical performance of the proposal in the paper is evaluated through an extensive simulation study in Section 6. Finally, some conclusions are drawn in Section 7.

2. LOCAL LINEAR ESTIMATION OF THE INTENSITY FUNCTION AND IT FIRST DERIVATIVE

2.1. Model and local linear estimators

This paper is concerned with nonparametric estimation of the intensity of a counting process, $\{N(t); t \geq 0\}$. The conditional rate or intensity function of a counting process $\{N(t); t \geq 0\}$ is defined as

$$\lambda(t) = \lim_{\Delta \to 0} \frac{Pr\left\{N(t+\Delta) - N(t) \geq 1 | F_{t^-}\right\}}{\Delta}, \tag{1}$$

where F_{t^-} is a filtration which describes the history of the process up to, but not including, time t. The filtration F_{t^-} is generated by the set $\{N(s); 0 < s < t\}$, and so, it contains all the information about event arrivals in the past, that is until t.

In the general case, the intensity is a stochastic function. Aalen[5] suggested a multiplicative model by assuming that the conditional rate defined in equation (1) has the form $\lambda(t) = \alpha(t)Y(t)$, with α being an unknown non-negative deterministic function and Y a non-negative observable stochastic process whose value at any time t is known just before t, so Y is a predictable process.

In many cases Y is the so-called *at risk*, process, i.e. $Y(t)$ takes value 1 when the subject is under observation at time t, and 0 otherwise. The intensity function of a NHPP is a particular case satisfying the Aalen's multiplicative model for which $Y(t) = 1$, for all t in the interval of duration of the experiment. In other words, $\lambda(t) = \alpha(t)$, for all $t \geq 0$. A Cox-type model may also be encompassed by defining $Y(t) = \exp(\beta^\top \mathbf{X}_i(t))$, with $\mathbf{X}_i(t)$ a covariate process for subject i.

Consider that we observe a sample of n systems and let N_i count observed failures for the ith individual in the time interval $[0, T]$, $\{N_i(t), t \in [0, T]\}$ is a counting process, for $i = 1, \ldots, n$. For each, we assume the Aalen's multiplicative model so that the random intensity is written as $\lambda_i(t) = \alpha(t)Y_i(t)$, with no restriction on the functional form of the hazard function $\alpha(\cdot)$, and Y_i is a non-negative predictable process, finally $(N_1, Y_1), \ldots, (N_n, Y_n)$ are i.i.d. for the n systems in the sample.

Under a local linear approach we assume that, for each t, the hazard function $\alpha(t)$ can be locally approximated (in a neighborhood of t) by a linear function, this is, for all $s \in (t - h, t + h)$, $\alpha(t) = \theta_0 + \theta_1 (s - t)$, for an appropriate bandwidth h. Thus, at the time point t, an estimation of the intercept θ_0 would provide an estimation of $\alpha(t)$, whereas an estimation of the slope θ_1 would provide an estimation of the derivative $\alpha'(t)$.

To this goal, we formulate the following least squares problem (see Nielsen and Tanggaard[21]):

$$\left(\widehat{\theta}_0, \widehat{\theta}_1\right)^\top = \underset{(\theta_0, \theta_1)^\top}{\arg\min} \sum_{i=1}^{n} \int_0^T \left(\Delta N_i(t) - \theta_0 - \theta_1 (s - t)\right)^2 K_h (s - t)\, Y_i(s) ds, \tag{2}$$

where $K_h(\cdot) = K(\cdot/h)/h$, with K an appropriate kernel function. For simplicity let us denote $N(t) = \sum_{i=1}^n N_i(t)$ and $Y(t) = \sum_{i=1}^n Y_i(t)$, the aggregated processes, respectively. The solution to the problem (2) provides estimates for the hazard function and its first derivative, which can be expressed as follows:

- For the hazard function, $\widehat{\theta}_0 = \widehat{\alpha}(t)$:

$$\widehat{\alpha}_{LL}(t) = \int_0^T \frac{a_2(t) - a_1(t)(s - t)}{a_2(t)\, a_0(t) - (a_1(t))^2} K_h (s - t)\, dN(s). \tag{3}$$

- For the first derivative of the hazard, $\widehat{\theta}_1 = \widehat{\alpha}'(t)$:

$$\widehat{\alpha}'_{LL}(t) = \int_0^T \frac{a_0(t)(s - t) - a_1(t)}{a_2(t)\, a_0(t) - (a_1(t))^2} K_h (s - t)\, dN(s). \tag{4}$$

Here we have defined the moments a_j, for $j = 0, 1, 2$,

$$a_j(t) = \int_0^T (s - t)^j K_h (s - t)\, Y(s) ds. \tag{5}$$

2.2. Consistency and asymptotic normality

The pointwise asymptotic properties of the local linear estimator of intensity rate, given in (3), are obtained in Nielsen and Tanggaard[21]. The authors demonstrate that

$$\widehat{\alpha}_{LL}(t) - \alpha(t) = B_0(t) + V_0(t) \tag{6}$$

where $B_0(t) = \frac{1}{2}h^2\mu_2(K)\alpha''(t) + o_P\left(h^2\right)$ and, $(nh)^{1/2}V_0(t) \to N\left(0, \frac{R(K)\alpha(t)}{\gamma(t)}\right)$, with $\mu_j(K) = \int u^j K(u)du$, for $j = 0, 1, \ldots$, and, $R(K) = \int K^2(u)du$.
Now, to derive the pointwise asymptotic properties of the estimator of the derivative we proceed as in Nielsen and Tanggaard[21], that is, we split the error into a deterministic term $B(t)$ converging in probability plus a variable term $V(t)$ converging to a normal distribution. Using that $dN(t) = dM(t) + d\Lambda(t)$, where M is a martingale, and $\Lambda(t) = \int \alpha(t)Y(t)dt$ is a predictable process, the compensator for N, then we can write $\widehat{\alpha}'_{LL}(t) - \alpha'(t) = B(t) + V(t)$, where

$$V(t) = \int_0^T \frac{a_0(t)(s-t) - a_1(t)}{a_2(t)a_0(t) - (a_1(t))^2} K_h(s-t)\, dM(s), \tag{7}$$

and,

$$B(t) = \int_0^T \frac{a_0(t)(s-t) - a_1(t)}{a_2(t)a_0(t) - (a_1(t))^2} K_h(s-t)\,\alpha(s)Y(s)ds - \alpha'(t). \tag{8}$$

The following theorem provides the asymptotic behaviour of these terms.

Theorem 1. *Assume that the following conditions hold:*

A1. The bandwidth $h = h(n)$ satisfies $h \to 0$ and $nh^3 \to +\infty$, for $n \to +\infty$.

A2. The kernel K is symmetric, supported on the interval $[-1, 1]$ and with finite second moment.

A3. It holds that $\alpha \in C_2([0, T])$.

A4. There exists a function $\gamma \in C_1([0, T])$ such that it is strictly positive for $t \in [0, T]$, and that $\sup_{s\in[0,T]} |Y(s)/n - \gamma(s)| = o_P(1)$.

Then we have that

$$B(t) = o_P\left(h^2\right) \tag{9}$$

and

$$\left(nh^3\right)^{1/2} V(t) \xrightarrow{D} N\left(0, \sigma_t^2\right) \tag{10}$$

where $\sigma_t^2 = \frac{\alpha(t)\int_0^T u^2K^2(u)du}{\gamma(t)\mu_2^2(K)}$.

2.3. Inference on the NHPP rate based on aggregated data

The arrival rate of a NHPP can be considered as a particular case of Aalen's model, where $Y(t) = 1$ for all t in the interval of duration of the experiment. In other words, $\lambda(t) = \alpha(t)$, for all $t \geq 0$. We observe a sample of n arrival times $T_1 < T_2 < \ldots < T_n$. Thus, the sampling information consists of a single realization of a NHPP $\{N(t); t \geq 0\}$ and the goal is to obtain an estimate of the failure rate $\lambda(t)$. The failures occurring at disjointed intervals are assumed to be independent and there are no simultaneous failures in the system.

In applications in reliability engineering, this means that a single system is followed until a failure occurs, immediately the system is fixed and restored to work. After the repair the system's state is exactly the same as it was before failure. The "as-bad-as-old" condition after the failure/repair or, equivalently "minimal repair" maintenance is being carried out by the system environment.

Now we consider the local linear estimator of the rate of a NHPP when only the successive counts of failures at disjoint consecutive intervals of time are available. As a result we derive discretized versions of the estimators for the ROCOF and it first derivative presented in (3) and (4).

Under a discrete formulation the sampling information consists of counts of occurrences of the process at fixed time points $\{x_0 = 0, x_1, \ldots, x_M\}$, i.e. $N_r = \int_{x_{r-1}}^{x_r} dN(s)$, for $r = 1, \ldots, M$. As the process is NHPP, then N_r comes from a Poisson distribution with parameter $\mu_r = \Lambda(x_r) - \Lambda(x_{r-1})$, for $r = 1, \ldots, M$. Here Λ is the cumulative rate function, $\Lambda(t) = \int_0^t \lambda(u)du$. We can approximate $\mu_r \approx \lambda(x_r)(x_r - x_{r-1}) = \lambda_r \Delta_r$, where we denote $\lambda_r = \lambda(x_r)$, and $\Delta_r = x_r - x_{r-1}$, $r = 1, \ldots, M$.

For each x_r with $r = 1, \ldots, M$ and for each $j = 0, 1, 2$ we can approximate $a_j(x)$ by

$$a_{d,j}(x) = \sum_{m=0}^{M} (x_m - x_r)^j K_h(x_m - x_r) \Delta_m \tag{11}$$

so we can write the discrete version of the local linear estimator of the ROCOF as

$$\widehat{\alpha}_{d,h}(x_r) = \sum_{m=0}^{M} \left(\frac{A_2(x_r) - A_1(x_r)(x_m - x_r)}{A_2(x_r) A_0(x_r) - (A_1(x_r))^2} \right) K_h(x_m - x_r) \frac{N_m}{\Delta_m}, \tag{12}$$

and the first derivative

$$\widehat{\alpha}'_{d,h}(x_r) = \sum_{m=0}^{M} \left(\frac{A_1(x_r) - A_0(x_r)(x_m - x_r)}{A_2(x_r) A_0(x_r) - (A_1(x_r))^2} \right) K_h(x_m - x_r) \frac{N_m}{\Delta_m}, \tag{13}$$

where $A_j(x) = \sum_{m=0}^{M} (x_m - x)^j K_h(x_m - x)$, for $j = 0, 1, 2$.

Alternative expressions for the variance of the estimates can be easily computed from the expressions (12) and (13), instead of using discretized version of the variance obtained for the continuous case given in (10). Specifically, the variance of $\widehat{\alpha}'_{d,h}(x_r)$ can be directly deduced from the expression (13) as follows:

$$Var\left(\widehat{\alpha}'_{d,h}(x_r)\right) = \sum_{m=0}^{M} \left(\frac{A_1(x_r) - A_0(x_r)(x_m - x_r)}{A_2(x_r) A_0(x_r) - (A_1(x_r))^2} \right)^2 (K_h(x_m - x_r))^2 \frac{Var(N_m)}{\Delta_m^2}. \tag{14}$$

For each $m = 1, \ldots, M$, we have that $Var\left(N_m\right) = \lambda_m \Delta_m$, and then we can estimate the variance above using the empirical estimator of λ_m, $\widehat{\lambda}_m \approx N_m/\Delta_m$ $(m = 1, \ldots, M)$, so

$$\widehat{Var}\left(\widehat{\alpha}'_{d,h}\left(x_r\right)\right) = \sum_{m=0}^{M} \left(\frac{A_1\left(x_r\right) - A_0\left(x_r\right)\left(x_m - x_r\right)}{A_2\left(x_r\right) A_0\left(x_r\right) - \left(A_1\left(x_r\right)\right)^2} \right)^2 \left(K_h\left(x_m - x_r\right)\right)^2 \frac{N_m}{\Delta_m^2}. \tag{15}$$

3. THE SMOOTHING PARAMETER AND NONPARAMETRIC INFERENCE

The kernel estimators defined in the previous section involve an unknown bandwidth parameter that determines the level of smoothing to be considered. To illustrate the effect of the bandwidth on the estimated failure intensity we consider the classic coal mining disaster data. Details about these data are provided in Section 5.3. In such an industrial accident the aim is to explore the overall trend in the ROCOF (the rate of occurrence of explosions) trying to find a decreasing trend, but also looking for possible local trend changes. Figure 1 shows four estimates of the ROCOF function computed from these data. All of them are local linear kernel estimators derived from equation (12) but with different bandwidths, $h = 2, 10, 20$ and 50. The impression one can get looking at the estimates is quite different. While the smallest bandwidth produces many wiggles in the ROCOF, suggesting many local trend changes, the biggest bandwidth produce a smooth curve with a clear decreasing trend and no changes. On the other hand moderate bandwidths suggest both an overall decreasing trend but two bumps around 1880 and 1940, for $h = 20$, and even a third one around 1910 for $h = 10$.

The bandwidth effect we have visualized with this example is well known in kernel smoothing. Big bandwidths produce oversmooth estimates at the risk of smoothing away important features of the data. Too small bandwidths produce undersmooth estimates with too many wiggles. Choosing the bandwidth becomes then a bias-variance trade-off problem. When the aim of kernel smoothing is to provide a good estimator of the target function the common approach starts defining what is considered the "optimal" bandwidth, and then, since optimal bandwidths are infeasible in practice, specific methods are defined to find a proper estimate from the available data. The least-squares cross-validation method is maybe one of the simplest and most popular bandwidth selectors, which can be used for the kernel estimators considered in this paper (Brooks and Marron[24]). Other popular approaches for bandwidth selection are based on plug-in rules such as the method proposed by Chen *et al.*[22] for their local linear estimator. However, if the goal is beyond the pointwise estimation of the underlying curve and one wants to assess the significance of its features, a common way to proceed consist of deriving inferential conclusions based on a bandwidth choice. Such approach has been followed by Cowling *et al.*[23] who constructed bootstrap confidence intervals for the ROCOF of the coal mines data, based on a kernel estimator with a cross-validated bandwidth. However, since the kernel estimator is biased these confidence intervals estimate the expectation of the ROCOF, not the target ROCOF. The authors discuss how to correct for this bias but without providing any practical guidance (in fact in the coal mines example no bias correction was performed).

The inferential approach we adopt in this paper differs from the traditional approach where a single bandwidth is chosen and the inferential conclusions are drawn from a kernel

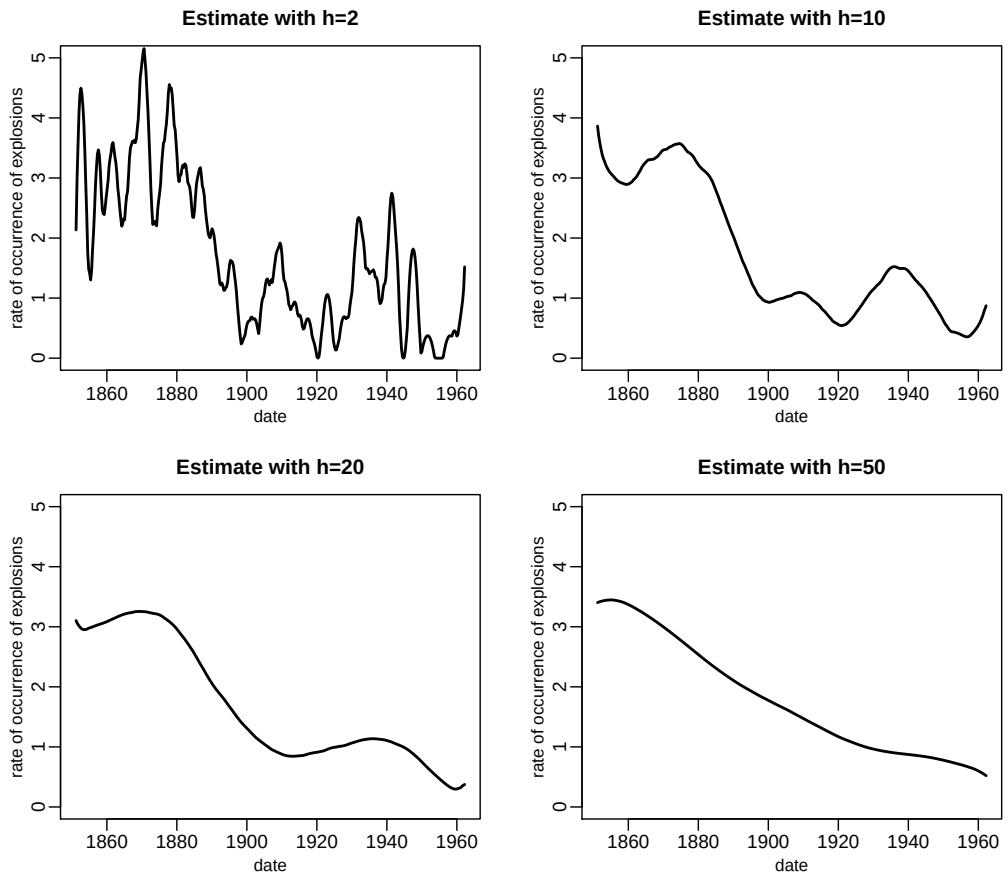

Figure 1: Effect of the bandwidth choice on the local linear estimates of the intensity (coal mines data).

estimator with such bandwidth. We consider nonparametric estimation from the viewpoint of "scale space theory" (Lindeberg[25], Chaudhuri and Marron[26]). We focus simultaneously on a wide range of values for the smoothing parameter, instead of trying to estimate the optimum amount of smoothing from the data. This is an effective approach from exploratory purposes since different levels of smoothing may reveal different useful information in the data. In this sense, the smoothing levels are comparable with variations in the levels of resolution or scales in a visual system. Large bandwidths provide a "macroscopic or distant vision", where one can hope to resolve only large scale features. Similarly small bandwidths provide a "microscopic vision" that can resolve small scale features (provided that we have a sufficient amount of informative data). Under this perspective the traditional approach of choosing a single bandwidth (according to an optimality criteria) becomes uninformative and even misleading. Looking at the problem at a unique scale would mean to ignore significant characteristics if this bandwidth is too big, or overestimating the number of changes in the trend of the target function when the chosen bandwidth is too small. Chaudhuri and Marron[14] implemented the scale space inference for density and regression functions

through the graphical tool SiZer. In the next section we extend SiZer for the inference on the ROCOF function in the context described in Section 2.

4. DEVELOPMENT OF SIZER FOR THE ROCOF

After being introduced by Chaudhuri and Marron[14], SiZer has become a powerful tool for conducting exploratory data analysis in many statistical frameworks. Given a set of noisy data, it helps the data analyst to distinguish between the structures that are "really there" and those that are due to sampling noise. This is achieved by an effective combination of statistical inference in scale space and visualization.

SiZer consists of two plots, the so-called "family plot", which that is a family of smoothers indexed by the bandwidth parameter, and the coloured map, which displays information about the significant positivity and negativity of the first derivative. The map visualize the inference about the first derivative in a two dimensional space with $n_{grid} \times n_h$ pixels, considering two equally spaced grids, one of size n_{grid} defining the localizations, and the other of size n_h for the scales (bandwidths). In this arrangement the portions of the display are colour coded as follows: blue if zero is greater than the upper confidence limit (significantly increasing), red if zero is less than the lower confidence limit (significantly decreasing), purple if zero is within the confidence limits (not significantly increasing or decreasing), and grey indicating regions where the data are too sparse to make statements about significance (the effective sample size defined below is less than 5).

As an illustration, and before entering in more details, we show in Figure 2 the SiZer that corresponds to the coal mining disaster data considered in the previous section and fully described in Section 5.3. The family plot in the top panel shows the estimated rate of occurrence of accidents (ROCOF) over time (localization space) with different bandwidths (scales). Small bandwidths, which correspond to high resolution visualization, produce irregular intensity estimates with several spurious changes in the trend as a result of the variability in the data. In this case the data set is small with 191 observations. In this case we have constructed the SiZer Map with bootstrap confidence intervals derived from 1000 bootstrap samples, the output for the other type of intervals is quite similar though. The SiZer Map shows a clear decreasing trend and no changes. This is the same conclusion obtained by Barnard[27] and Cox and Lewis[28]. These authors showed that an exponential model provides an accurate fit for the intensity rate. They concluded that a general decreasing trend is exhibited by the accident hazard rate with no trend changes with time.

Following Chaudhuri and Marron[14], the confidence intervals for the first derivative of the target function, which is $\alpha(t)$ in the context of this paper, have been defined as

$$\left(\widehat{\alpha}'_h(t) + q_{1-p/2}\sqrt{\widehat{Var}(\widehat{\alpha}'_h(t))}, \widehat{\alpha}'_h(t) + q_{p/2}\sqrt{\widehat{Var}(\widehat{\alpha}'_h(t))}\right), \tag{16}$$

where p is the significance level, and $q_{1-p/2}$, $q_{p/2}$ are appropriate quantiles.

Notice that in Section 2 we have described the main elements required for the inference about the ROCOF with SiZer. We consider the local linear estimator given in (3) to define the family of smoothers, and compute confidence intervals for the first derivative from expression (16), using the local linear estimator of the derivative given in (4), and

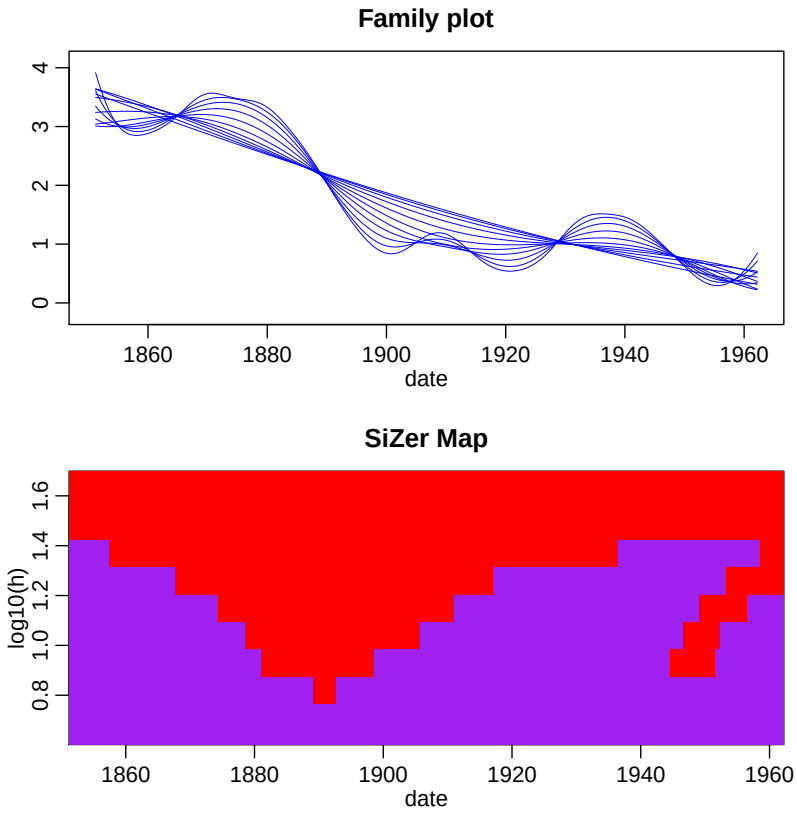

Figure 2: SiZer analysis of the coal mines data.

the estimate of its variance given in (15). It only remains how to calculate the quantiles $q_{1-p/2}, q_{p/2}$. We devote the rest of this section to define two different approaches, one based on the limiting normality property and other based on bootstrapping.

The pointwise asymptotic normality of these estimators given in Theorem 1 can be used to construct pointwise confidence intervals, just by taking $q_{1-p/2}$ and $q_{p/2}$ equal to the $(1-p/2)$ and $p/2$ quantiles of the standard Normal distribution, respectively.

Chaudhuri and Marron[14] pointed out that, even though the Normal approximation works fine, pointwise quantiles are not recommended in some cases where the map seems to suggest that too many features are "significant". SiZer is a simultaneous display of statistical inferences, so the multiple comparison problem can be addressed using simultaneous inference across the localizations.

Simultaneous inference for SiZer is solved by defining m independent confidence interval problems, where m reflects the number of independent blocks. Thus, the simultaneous Normal quantiles in SiZer are calculated as follows

$$q_{1-p/2} = -q_{p/2} = \Phi^{-1}\left(\frac{1+(1-p)^{1/m}}{2}\right). \tag{17}$$

Here Φ^{-1} is the quantile function standard Normal law and m, which depends on the bandwidth h, $m \equiv m(h)$, is the number of independent blocks of average size available from a dataset of size n. The estimation of m is based on an estimate of the effective sample size (ESS), which reflects the "number of data points in each kernel window".

For the kernel estimator of the intensity function the ESS can be computed as

$$ESS(t,h) = \frac{\sum_{i=1}^{n} \int_0^T K_h(t-s)dN_i(s)}{K_h(0)}. \tag{18}$$

And the number of independent blocks for each h is estimated as:

$$m = \frac{n}{avg_{t\epsilon\mathcal{D}_h} ESS(t,h)} \tag{19}$$

where $avg_{t\epsilon\mathcal{D}_h}$ denotes the average value on the set $\mathcal{D}_h = \{t : ESS(t,h) \geq 5\}$.

As an alternative to the Normal confidence intervals proposed above, the bootstrap method can be used to construct pointwise and simultaneous confidence intervals. We consider percentile-t bootstrap confidence intervals based on one of the resampling methods suggested by Cowling *et al.*[23], we refer the reader to this paper for a detailed description of the resampling method (named as method 2) as well as the derived percentile-t intervals, also Gámiz *et al.*[29] (pp. 80). Simultaneous bootstrap confidence intervals can be derived using again the independent blocks approach and the ESS described above.

The four types of intervals defined above have been considered and compared in the empirical analyses reported in the next sections.

5. APPLICATION TO REAL DATA

5.1. Preamble

For illustration we have included in 5.2-5.5 the analysis of four real data examples. We begin our study checking whether the Poisson assumption is admissible for the underlying process that governs the arrivals in all the examples presented in this section. To do so we have considered a graphical check similar to the one in Gámiz and Lindqvist[30]. Specifically, if the occurrence process is a NHPP, the transformation of the successive event times by means of the cumulative intensity function will provide successive arrival times according to a homogeneous Poisson process with rate 1 on the transformed scale. To obtain the interarrival times on the transformed scale, we have previously calculated a nonparametric estimator of the intensity function using the procedure presented in Gámiz and Lindqvist[30].

If the underlying process is a NHPP, these times are independent and identically distributed as an Exponential law of rate 1 and then the corresponding hazard estimation should be around the line $y = 1$.

The procedure we have implemented to construct the plots for the corresponding visual check of the Poisson hypothesis can be summarized as follows:

- The time sequence between successive arrivals on the transformed scale is calculated as $X_i = \widehat{\Lambda}(T_i) - \widehat{\Lambda}(T_{i-1})$ with $i = 1, \ldots, n$.

- If the arrival process on the original scale is a NHPP, then the $\{X_1, \ldots, X_n\}$ are independent and identically distributed according to an exponential law with rate 1.
- Estimate the hazard of $\{X_1, \ldots, X_n\}$ and compare with the line $y = 1$.

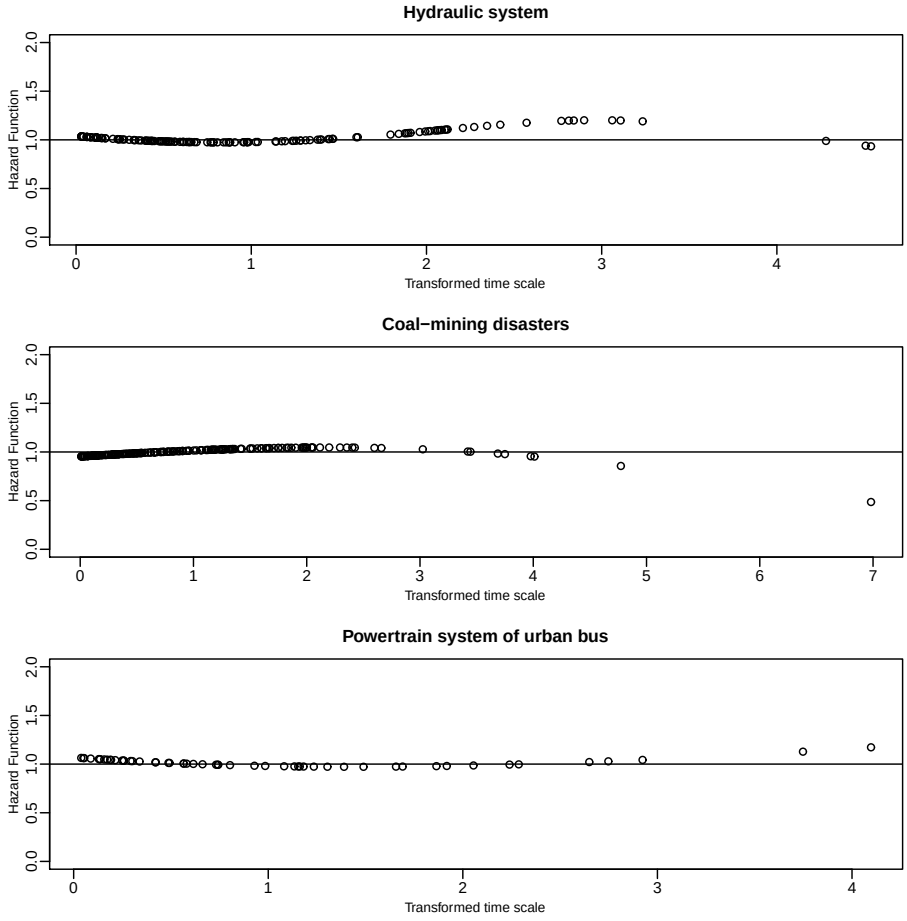

Figure 3: Visual check of the Poisson assumption for the three analysed datasets: Hydraulic system, Coal-mining disasters, Powertrain system of a city bus.

5.2. Hydraulic system of load-haul-dump machines

Here we describe an application in reliability engineering. The data have been taken from Kumar and Klefsjö[31] and consist of the times between successive failures (in hours, and excluding repair or down times) of the hydraulic systems of the load-haul-dump (LHD) machines selected for the study (six individual machines in total). The authors conclude in their analysis that the failure times of each item (machine) can be adequately represented by a NHPP. Given that machines operate independently each other in time, we can consider

the overall failure process, that is all failures occurred in all items, also as a NHPP. This fact is confirmed by the visual check we present on the top panel of Figure 3.

We have then performed the SiZer analysis for these data and shown the result in Figure 4. Looking at the family plot we can see that small bandwidths (high resolution levels) produce many wiggles on the underlying intensity (the rate of occurrence of failures, ROCOF), while large bandwidths (low resolution visualization) tends to hide many of the characteristics proving a nearly decreasing trend. The question is then whether the characteristics shown in the family plot are indeed significant. The colour map below provides a statistical answer to this question at the nominal level 5%. Specifically it shows at each pixel (time and bandwidth) which is the sign of the intensity derivative with 95% confidence. Reading the map (from left to right and taking into account the colour code described above) we can conclude that the ROCOF is significant increasing up to about 1800 hours and it decreases afterwards. The colour change blue-purple-red around 2000 hours means that the ROCOF exhibits a significant trend change (a bump) at that time. Finally we can see that this trend change can be visualized at most of the considered bandwidths.

The SiZer map shown in Figure 4 have been constructed using simultaneous bootstrap intervals (with 1000 bootstrap samples). The results are quite close for the other types of intervals, however the bootstrap method seems to be appropriate for these data since the sample size is small, just 151 observations.

5.3. Coal data

In this example, we consider the data concerning to mining accidents (explosions) caused by coalbed gas or coal dust that caused the deaths of 10 or more miners during many years. The data are taken from Jarrett[32] and consists of 191 times of occurrences of accidents (in days) occurring during a period from March 15, 1851 to March 22, 1962. Source: package *boot* in R. The occurrences of such accidents can be considered as a NHPP (see Figure 3). The interest of this example arises from the need to know possible patterns of occurrence of accidents to a better comprehension of the nature of such events. We have then performed the SiZer analysis for this dataset and the results are shown in Figure 2 (see Section 4). The plots show that the ROCOF is decreasing with no changes in trend. This characteristic in the ROCOF curve can be clearly visualized for all the scales (smoothing parameters) considered in the plot. In this case we have considered again simultaneous bootstrap intervals (with 1000 bootstrap samples).

5.4. Powertrain system of an urban route bus

In this case the data have been taken from Guida and Pulcini[33] and consist of 55 failure times (in kilometres) of the powertrain system of an urban route bus between the early months of 1999 and up to the end of December of 2004. Each powertrain system was subject to minimal repair at failure which is corroborated by our graphical check of the Poisson assumption (see bottom panel in Figure 3).

The bus was circulating on urban roads of the city of Naples. The powertrain of the bus consists of a FIAT engine, transmission ZF gearbox, driveshafts and differentials. The powertrain system was subject to minimum repair after the failure due to three factors:

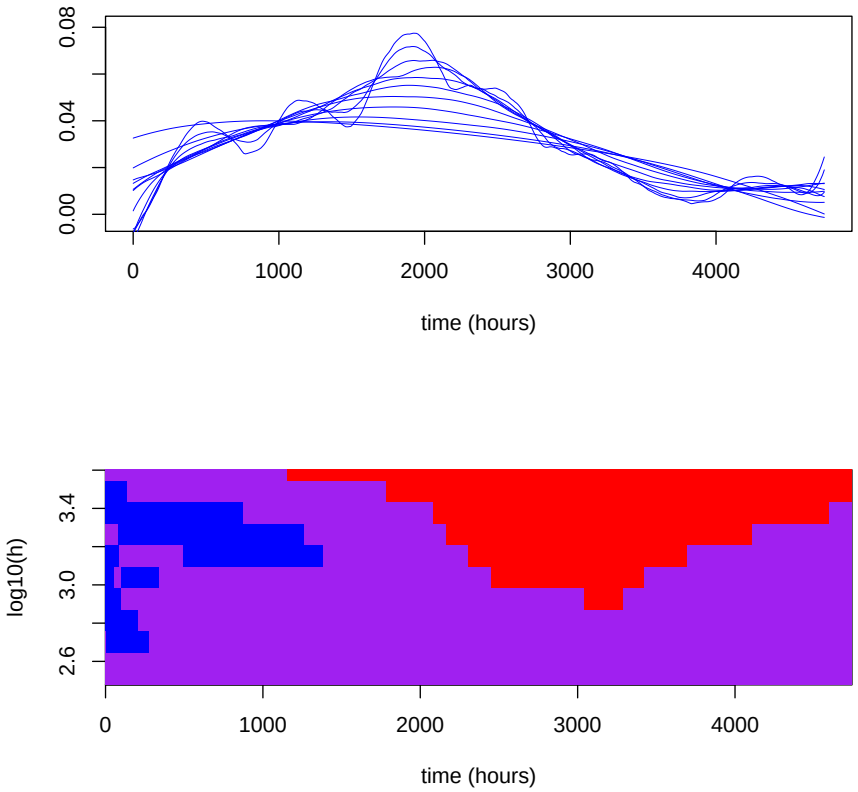

Figure 4: SiZer analysis of the hydraulic system data.

a) the complexity of the system, b) the expected presence of premature failure, and c) the large number of failures/repairs experienced during the whole observation period. In this example we are interested in exploring failure patterns of the powertrain system of these buses.

SiZer analysis for this dataset is shown in Figure 5. A close inspection to these plots reveals that the ROCOF presents three significant changes. The map displays a colour change red-purple-blue between 0 and 150 kilometres, which means that the ROCOF exhibits a significant decreasing tendency of the failure during the first part of the bus lifetime at that time. The colour change blue-purple-red between 150 and 250 kilometres means that the ROCOF also exhibits a significant trend change at that time, and the colour change red-purple-blue between 300 and 400 kilometres means that the ROCOF exhibits a significant trend change at that time. These characteristics of the ROCOF are displayed at all resolution levels, this is, for all the bandwidths considered in the plot.

As conclusion our analysis detects a peak in the ROCOF, meaning a trend change in the failure occurrences approximately after 200 kilometres of use. This feature is not reflected by the parametric approach developed in the paper of Guida and Pulcini [33].

The SiZer map shown in Figure 5 has been constructed using pointwise Normal intervals.

The results for the other types of intervals are quite close though.

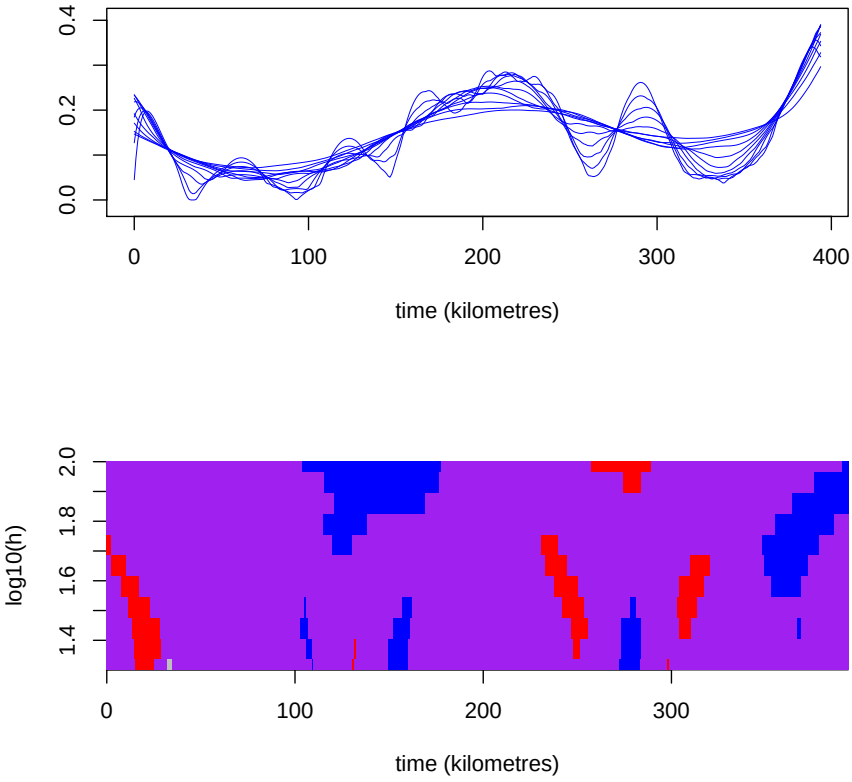

Figure 5: SiZer analysis of the powertrain system of a city bus.

5.5. Storm occurrences in the Artic Sea

Unlike the previous examples, in this case we do not have information about the exact times of occurrences, instead we have monthly counts of the event of interest.

Our main concern in this example is to explore cyclic behaviour of the intensity of the underlying NHPP. The data we consider have been taken from Lee *et al.*[34] and consist of oceanic high-wave events, which are referred as storms. These events were observed each month over a nine-year observation interval, at an off-shore drilling site in the Artic Sea. A total of 302 storms were observed during this time interval. According to Lee *et al.*[34] the observed series of storm-arrival times has pronounced cyclic behaviour, and the rate of occurrence of these events appears to vary smoothly from year to year.

In their analysis, the authors conclude that there are strong evidence against the hypothesis that the storm-arrival process is a homogeneous Poisson process. They argue that there are good reasons to believe that the storm-arrival process will exhibit a pronounced time-of-year effect. In consequence they propose a parametric model for the intensity function in terms of an exponential-polynomial-trigonometric function that provides a good

explanation of the cyclic event arrivals. Our SiZer analysis supports their conclusions as we describe below.

The results of the SiZer analysis are displayed in Figure 6. The family plot shows that the observed series of storm-arrival times has pronounced cyclic behaviour, where the peaks are produced in the middle of each year, that is, the frequency of the storms is higher at midyear. All these peaks are concluded to be significant in the map, this can be shown in the colour changes blue-purple-red that occurs around the middle of each year period (one peak per year). These plots have been constructed using pointwise intervals based on the Normal approximation. This choice is based on the sample size of this dataset and the high frequency in the underlying ROCOF, which can be noticed looking at the family plot in the first graph of Figure 6.

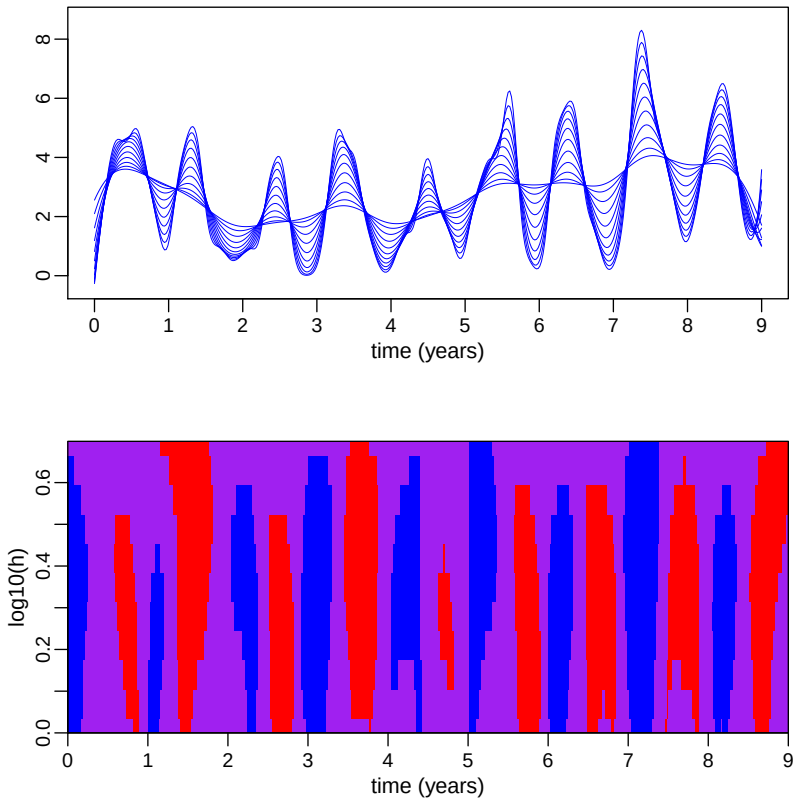

Figure 6: SiZer analysis based on the Artic Sea high-wave events.

6. SIMULATION STUDY

The main purpose of this section is to elucidate the effectiveness of our procedure based on the SiZer analysis, when evaluating the underlying shape of the ROCOF of a repairable

system. Then, we focus just on the deterministic part of the intensity function and we set $Y(t) = 1$, for all the simulations below. In other words, in all cases we simulate data from an NHPP, for which $\lambda(t) = \alpha(t)$.

We consider four theoretical models with rate functions and sample sizes summarized in Table 1 and plotted in Figure 7. The two first models represent intensities that do not show any change in the trend but a constant trend (M1), or an increasing monotone trend (M2). The third model shows two changes in the trend and the fourth model is a high frequency signal, which exhibits thirteen changes in the trend.

Table 1: Simulated models.

Model	Rate function	Sample size n
M1	$\lambda_1(t) = 1$	100
M2	$\lambda_2(t) = 3t^2$	500
M3	$\lambda_3(t) = 100 + 50\cos\left(\frac{1}{2}\pi t\right)$	500
M4	$\lambda_4(t) = 100 + 50\cos\left(\frac{3}{2}\pi t\right)$	1000

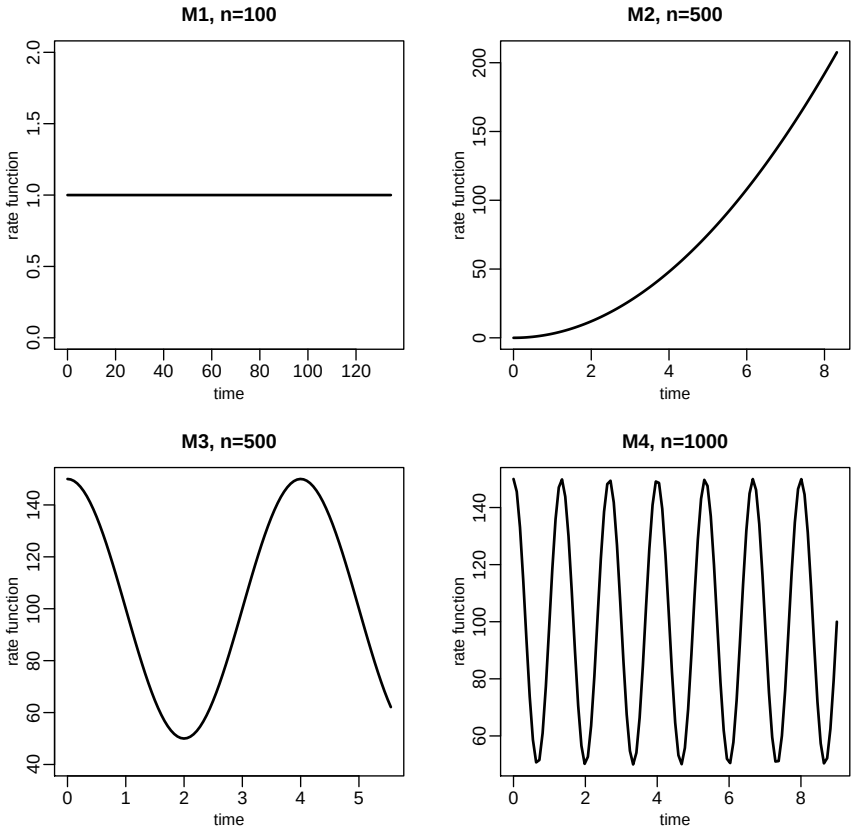

Figure 7: Rate functions for the models and sample size considered.

From each model we have simulated 1000 samples as follows. For $i = 1, \ldots, n$, we generate u_i from a uniform distribution in $[0, 1]$, then we define $x_i = -\log u_i$ and $r_i =$

$r_{i-1} + x_i$, with $r_0 = 0$. Finally the occurrence times t_i, are defined as $t_i = \Lambda^{-1}(r_i)$, with $\Lambda(t)$ being the cumulative rate function.

The ROCOF and its first derivative have been estimated using the local linear estimators defined in Section 2, with Epanechnikov kernel.

The SiZer maps have been constructed to visualize the inference about the first derivative of the intensity rate in a two dimensional space with 401×11 pixels. This has been defined using two equally spaced grids, one of size 401 defining the localizations (times), and the other of size 11 defining the scales or resolution levels (bandwidths). The localizations have been defined between suitable minimum and maximum values that contain, for each model, all the generated times. The minimum and maximum values to define the grid of bandwidths have been chosen, for each model, to allow a suitable visualization of the inference problem at both low and high resolution level. Finally we have considered and compared four types of confidence intervals to construct the SiZer maps. These are the obtained using Normal or bootstrap intervals, and pointwise or simultaneous inference as described in Section 3. The computational complexity of the bootstrap method has been addressed by using parallel programming in R (R Core Team[35]), and restricting the number of bootstrap samples to 500 in the simulation (whereas it was 1000 in the real data analyses described in the previous section).

With the above specifications we now evaluate the capability of SiZer to detect the true number of trend changes in the ROCOF. To this goal we have counted the number of changes detected from inspecting the SiZer map, from each of the 1000 simulated samples. Tables 2 to 5 summarize the results for models M1 to M4, respectively. Each table shows the results for the 11 considered bandwidths (represented by columns in logarithmic scale) and for each type of confidence intervals (Normal and bootstrap, pointwise and simultaneous). For all cases, the counts for each column adds up to 1000, except for few cases where the bandwidth was too small for some simulated samples to make valid inference, and they were discarded.

Model M1 corresponds to a constant rate and therefore no significant changes should be detected. In the second column of Table 2 we have written the number of changes detected by SiZer along the 1000 samples. The true number of changes is highlighted in the shaded row. Note that the simultaneous inference is the more appropriate in this case, almost all samples are detecting no changes for all bandwidths. As expected with a sample size of $n = 100$, the bootstrap intervals provide better results than those derived from the Normal approximation. On the other hand, pointwise intervals tend to show few changes over time, and specially for small bandwidths. Similar results can be seen for model M2 in Table 3, where the rate function is strictly increasing. However, in this case, the pointwise intervals provide quite good results too, being able to detect zero changes from most of the simulated samples.

The results are quite different for complex models with several changes as models M3 and M4. For model M3, which exhibits two changes, the summary in Table 4 shows that the pointwise intervals are able to detect the two changes in most of samples, specially with moderate bandwidths. For the high frequency model M4, thirteen changes should be detected by SiZer. Table 5 shows that, using simultaneous intervals SiZer fails, detecting less characteristics for many of the simulated samples. These poor results can be seen with

all bandwidths. On the contrary, the pointwise intervals are able to detect the true number of changes in most of the samples, and specially with moderate bandwidths. In this case both Normal and bootstrap intervals give similar results, as expected with a sample size of $n = 1000$.

Table 2: Number of trend changes in the ROCOF detected by SiZer in 1000 simulated samples from model M1. The true number of changes corresponds to the shaded rows.

Model M1	Changes \ $\log_{10}$(h)	1.00	1.05	1.10	1.14	1.19	1.24	1.29	1.33	1.38	1.43	1.48
Pointwise Normal	0	701	744	769	790	804	835	860	869	822	794	742
	1	230	206	196	172	167	147	129	122	171	202	250
	2	59	42	33	37	29	18	11	9	7	4	8
	3	9	8	2	1	0	0	0	0	0	0	0
	4	1	0	0	0	0	0	0	0	0	0	0
Simultaneous Normal	0	987	981	979	979	980	975	973	969	944	926	870
	1	10	18	20	19	19	24	27	31	56	74	130
	2	3	1	1	2	1	1	0	0	0	0	0
Pointwise bootstrap	0	461	534	589	630	670	724	762	783	743	705	658
	1	347	322	314	295	272	239	217	201	242	283	326
	2	149	120	88	73	57	37	21	16	15	12	16
	3	39	23	9	2	1	0	0	0	0	0	0
	4	4	1	1	0	0	0	0	0	0	0	0
Simultaneous bootstrap	0	1000	1000	1000	1000	1000	1000	1000	1000	1000	999	992
	1	0	0	0	0	0	0	0	0	0	1	8

Table 3: Number of trend changes in the ROCOF detected by SiZer in 1000 simulated samples from model M2. The true number of changes corresponds to the shaded rows.

Model M2	Changes \ $\log_{10}$(h)	-0.10	-0.06	-0.02	0.02	0.06	0.10	0.14	0.18	0.22	0.26	0.30
Pointwise Normal	0	998	1000	1000	1000	1000	1000	1000	995	980	936	820
	1	0	0	0	0	0	0	0	5	20	64	180
	2	2	0	0	0	0	0	0	0	0	0	0
Simultaneous Normal	0	1000	1000	1000	1000	1000	1000	1000	996	986	963	873
	1	0	0	0	0	0	0	0	4	14	37	127
Pointwise bootstrap	0	993	997	999	1000	1000	1000	997	994	973	914	785
	1	2	1	0	0	0	0	3	6	27	86	215
	2	5	2	1	0	0	0	0	0	0	0	0
Simultaneous bootstrap	0	1000	1000	1000	1000	1000	1000	1000	1000	1000	997	995
	1	0	0	0	0	0	0	0	0	0	3	5

7. CONCLUDING REMARKS

In this paper the main focus has been nonparametric inference about the failure rate (ROCOF) of a repairable system from the viewpoint of "scale space theory". We have assumed for the system behaviour a counting process under the Aalen's multiplicative intensity model. To derive the inference conclusions we have focused simultaneously on a wide range of values for the smoothing parameter instead of trying to estimate the optimum amount of smoothing from the data, as the traditional nonparametric inferential approach does. This is an effective approach from an exploratory point of view since different levels of smoothing may reveal different useful information in the data.

We have analysed several real datasets where our proposal based on a SiZer analysis has demonstrated to be a helpful tool to detect underlying structures in the shape of the

Table 4: Number of trend changes in the ROCOF detected by SiZer in 1000 simulated samples from model M3. The true number of changes corresponds to the shaded rows.

Model M3	Changes \ $\log_{10}$(h)	-0.30	-0.26	-0.22	-0.18	-0.14	-0.09	-0.05	-0.01	0.03	0.07	0.11
Pointwise Normal	0	0	0	0	0	0	0	0	0	0	0	1
	1	35	18	13	3	2	0	0	0	0	0	0
	2	961	982	987	997	998	1000	1000	1000	1000	1000	999
	3	4	0	0	0	0	0	0	0	0	0	0
Simultaneous Normal	0	10	3	1	0	0	0	0	0	0	0	0
	1	113	52	18	5	1	0	0	0	0	0	2
	2	877	945	981	995	999	1000	1000	1000	1000	1000	998
Pointwise bootstrap	0	1	0	0	0	0	0	0	0	0	0	0
	1	27	15	9	3	1	0	0	0	0	0	0
	2	966	983	991	997	999	1000	1000	1000	1000	1000	1000
	3	6	2	0	0	0	0	0	0	0	0	0
Simultaneous bootstrap	0	227	90	30	6	6	1	1	0	0	0	0
	1	609	608	487	318	209	100	48	23	9	14	24
	2	164	302	483	676	785	899	951	977	991	986	976

ROCOF. The simulation experiments have confirmed the effectiveness of SiZer to detect significant trend intensity changes.

Theorem 1 in Section 2 is valid for the general case of a counting process with the multiplicative intensity condition of Aalen. However, in the simulations (Section 6) we have concentrated on the NHPP case because we wanted to reproduce as close as possible the scenarios that we found in the real datasets that we have analyzed in Section 5. This is also the reason to choose the parametric models presented in Section 6 which, furthermore, represent a wide variety of real cases: from the simplest case of no trend changes to the most complex one where many trend changes in the intensity shape are observed. The Aalen' model has largely demonstrated to be very useful in applications, however there are, certainly, many cases where the intensity function of the failure process does not fit the Aalen' multiplicative model. In the case that the multiplicative structure of the Aalen model can not be assumed, the local linear estimation problem of the rate function, as well as its first derivative, has to be solved from a different point of view and the elements needed to construct the SiZer will require future research.

The SiZer analyses reported in this paper have been produced using self-programmed code in a form an R package that will be available at the CRAN site in the next months.

ACKNOWLEDGEMENTS

The authors are grateful for constructive comments from two reviewers and the Editor. This work has been partially supported by the Spanish Ministry of Economy and Competitiveness, through grants number MTM2013-41383P, MTM2016-76969P and ECO2013-48413-R, which include support from the European Regional Development Fund (ERDF). The authors thank Centro de Servicios de Informática y Redes de Comunicaciones (CSIRC), University of Granada, for providing the computing time.

Table 5: Number of trend changes in the ROCOF detected by SiZer in 1000 simulated samples from model M4. The true number of changes corresponds to the shaded rows.

Model M4	Changes \ $\log_{10}$(h)	-0.70	-0.64	-0.59	-0.54	-0.48	-0.43	-0.37	-0.32	-0.26	-0.21	-0.15
Pointwise Normal	5	1	0	0	0	0	0	0	0	0	0	0
	6	5	0	0	0	0	0	0	0	0	0	6
	7	32	8	5	0	1	0	0	0	0	1	3
	8	36	17	2	0	0	0	0	0	0	4	80
	9	141	68	37	17	9	4	2	1	1	6	71
	10	88	43	25	22	7	5	5	9	12	92	321
	11	309	312	230	177	142	69	43	24	27	59	88
	12	82	85	81	73	73	62	85	201	459	747	426
	13	303	466	616	707	760	838	768	571	264	29	3
	14	0	0	3	3	8	22	97	192	234	60	1
	15	3	1	1	1	0	0	0	2	3	2	0
Simultaneous Normal	0	430	148	34	9	1	0	0	0	0	0	0
	1	312	264	106	28	10	0	0	0	0	0	0
	2	162	249	184	75	21	0	0	0	0	0	5
	3	70	181	217	154	54	3	1	0	0	0	17
	4	21	102	183	155	91	12	2	1	1	3	68
	5	3	36	143	180	152	30	5	2	1	9	86
	6	2	15	70	132	119	57	15	5	10	48	212
	7	0	4	44	125	207	137	51	20	19	43	142
	8	0	1	13	71	120	119	72	59	82	159	256
	9	0	0	4	48	129	212	126	75	55	79	85
	10	0	0	2	15	50	121	161	208	287	381	102
	11	0	0	0	6	36	197	250	198	109	59	11
	12	0	0	0	2	4	47	138	268	366	218	16
	13	0	0	0	0	6	65	179	163	68	1	0
	14	0	0	0	0	0	0	0	1	2	0	0
Pointwise bootstrap	5	0	0	0	0	0	0	0	0	0	0	1
	6	0	0	0	0	0	0	0	0	0	0	4
	7	2	0	0	0	0	0	0	0	0	0	6
	8	4	1	0	0	0	0	0	0	0	3	61
	9	31	11	7	3	3	1	1	0	0	7	65
	10	18	15	7	4	4	5	3	3	9	62	286
	11	221	162	136	95	63	45	20	12	16	49	89
	12	77	64	55	47	51	45	71	178	415	763	482
	13	627	739	790	846	870	865	752	526	246	30	2
	14	5	3	3	4	9	39	153	277	309	83	4
	15	15	5	2	1	0	0	0	4	5	3	0
Simultaneous bootstrap	0	978	883	694	453	250	53	6	2	2	4	54
	1	21	93	225	300	276	87	15	8	4	18	126
	2	1	24	58	158	208	163	53	32	16	51	200
	3	0	0	20	59	146	186	96	37	52	90	212
	4	0	0	3	27	70	169	137	87	89	152	191
	5	0	0	0	2	36	140	156	103	94	160	99
	6	0	0	0	1	5	84	177	173	186	180	77
	7	0	0	0	0	6	69	139	148	138	128	25
	8	0	0	0	0	2	19	92	175	194	134	15
	9	0	0	0	0	1	24	77	102	89	37	1
	10	0	0	0	0	0	5	29	77	88	36	0
	11	0	0	0	0	0	1	18	33	23	4	0
	12	0	0	0	0	0	0	4	17	23	6	0
	13	0	0	0	0	0	0	1	6	2	0	0

REFERENCES

1. Ascher H, Feingold H. *Repairable systems reliability: modeling, inference, misconceptions and their causes*. New York: Marcel Dekker Inc; 1984.

2. Cha JH, Finkelstein M. *Point processes for reliability analysis. Shocks and repairable systems*. Springer; 2018.

3. Lindqvist BH, Elvebakk B, Heggland K. The trend-renewal process for statistical analysis of repairable systems. *Technometrics*. 2003;45:31–44.

4. Lindqvist BH. On the statistical modelling and analysis of repairable systems. *Stat Sci*. 2006;21:532–551.

5. Aalen OO. Non-parametric inference for a family of counting processes. *Ann Stat*. 1978;6:701–726.

6. Andersen PK, Borgan O, Gill RD, Keiding N. *Statistical models based on counting processes*. New York: Springer-Verlag; 1993

7. Krivtsov VV. Practical extensions to NHPP application in repairable system reliability analysis. *Reliab Eng Syst Safe*. 2007;92(5):560–562.

8. Wang FK, Lu YC. A New Model for Repairable Systems with Nonmonotone Intensity Function. *Qual Reliab Engng Int*. 2015;31:1553–1563.

9. Na MH, Jeon J, Park DH. Testing whether failure rate changes its trend with unknown change points *J Stat Plan Infer*. 2005;129:317–325

10. Garcia-Escudero LA, Fernandez MA, Duque O, Zorita AL. Warning procedures for systems that are improving. *Qual Reliab Engng Int*. 2008;24:377-387.

11. Louit DM, Pascual R, Jardine AKS. A practical procedure for the selection of time-to-failure modeling based on the assessment of trends in maintenance data. *Reliab Eng Syst Safe*. 2009;94:1618–1628

12. Taghypour S, Banjevic D. Trend analysis of the power-law process using Expectation-Maximization algorithm for data censored by inspection intervals. *Reliab Eng Syst Safe*. 2011;96:134–1348.

13. Phillips MJ. Estimation of the expected ROCOF of a repairable system with bootstrap confidence region. *Qual Reliab Engng Int*. 2001;17:159–166.

14. Chaudhuri P, Marron JS. SiZer for exploration of structure in curves. *J Am Stat Assoc*. 1999;94:807–823.

15. Marron JS, de Uña Álvarez J. SiZer for length biased, censored density and hazard estimation. *J Stat Plan Infer*. 2004;121:149–161.

16. Godtliebsen F, Oigard TA. A visual display device for significant features in complicated signals. *Comput Stat Data An.* 2005;48:317–343.

17. González-Manteiga W, Martínez-Miranda MD, Raya-Miranda R. SiZer Map for inference with additive models. *Stat Comput.* 2008;18:297–312.

18. Martínez-Miranda MD, Raya-Miranda R, González-Manteiga W, González-Carmona A. A bootstrap local bandwidth selector for additive models. *J Comput Graph Stat.* 2008;17:38–55.

19. Park C, Hernandez-Campos F, Le L, Marron JS, Park J, Pipiras V, Smith FD, Smith RL, Trovero M, Zhu Z. Long Range Dependence Analysis of Internet Traffic. *J Appl Stat.* 2011;38:1407–1433.

20. Park C, Hannig J, Kang K-H. Nonparametric Comparison of Multiple Regression Curves in Scale-Space. *J Comput Graph Stat.* 2014;23:657–677.

21. Nielsen JP, Tanggaard C. Boundary and bias correction in kernel hazard estimation. *Scand J Stat.* 2001;28:675–698.

22. Chen F, Yip PSF, Lam KF. On the Local Polynomial Estimators of the Counting Process Intensity Function and its Derivatives. *Scand J Stat.* 2011;38:631–649.

23. Cowling A, Hall P, Phillips MJ. Bootstrap confidence regions for the intensity of a Poisson point process. *J Am Stat Assoc.* 1996;91:1516–1524.

24. Brooks MM, Marron JS. Asymptotic optimality of the least-squares cross-validation bandwidth for kernel estimates of intensity functions. *Stoch Proc Appl.* 1991;38:157–165.

25. Lindeberg T. *Scale-Space Theory in Computer Vision.* Boston: Kluwer; 1994.

26. Chaudhuri P, Marron JS. Scale space view of curve estimation. *Ann Stat.* 2000;28:402–428.

27. Barnard, GA. Time intervals between accidents - a note on Maguire, Pearson and Wynn's paper. *Biometrika.* 1953;40:212–213.

28. Cox DR, Lewis PAW. *The Statistical Analysis of Series of Events.* Methuen, London; 1966.

29. Gámiz ML, Kulasekera KB, Limnios N, Lindqvist BH. *Applied nonparametric Satistics in Reliability.* Springer, London; 2011.

30. Gámiz ML, Lindqvist BH. Nonparametric estimation in trend-renewal processes. *Reliab Eng Syst Safe.* 2016;145:38–46.

31. Kumar U, Klefsjö B. Reliability analysis of hydraulic system of LHD machines using the power-law process model. *Reliab Eng Syst Safe.* 1992;35:217–224.

32. Jarrett RG. A note on the intervals between coal-mining disasters. *Biometrika*. 1979;66:191–193.

33. Guida M, Pulcini G. Reliability analysis of mechanical systems with bounded and bathtub shaped intensity function. *IEEE T Reliab*. 2009;58(3):432–443.

34. Lee S, Wilson JR, Crawford MM. Modeling and simulation of a nonhomogeneous Poisson process having cyclic behavior. *Commun Stat B-Simul*. 1991;20(2&3):777–809.

35. R Core Team (2017). R: A language and environment for statistical computing. R Foundation for Statistical Computing, Vienna, Austria. URL `https://www.R-project.org/`.

36. Ramlau-Hansen H. Smoothing counting process intensities by means of kernel functions. *Ann Stat*. 1983;11:453–466.

Appendix A. PROOF OF THEOREM 1

To demonstrate the asymptotic behavior of the hazard estimate we make use of the following central limit theorem for martingales which is presented as Proposition 4.2.1 in Ramlau-Hansen[36]:

Proposition in Ramlau-Hansen (1983, pp. 461). *Consider a predictable process* $W_n(t)$ *and assume that for some* $\sigma^2 > 0$

$$\int W_n^2(s)\alpha(s)Y(s)ds = \sigma^2 + o_P(1), \quad \int W_n^2(s)I\left\{W_n^2(s) > \epsilon\right\}\alpha(s)Y(s)ds = o_P(1),\ \epsilon > 0,$$

then, it holds that $\int W_n(s)dM(s) \xrightarrow{D} N\left(0, \sigma^2\right)$, *as* $n \to +\infty$.

First we study the bias term, $B(t)$. To do so, we consider a second order Taylor expansion of the rate function, that is, for $s \in (t-h, t+h)$,

$$\begin{aligned} B(t) = \int_0^T \frac{a_0(t)(s-t) - a_1(t)}{a_2(t)a_0(t) - a_1^2(t)} K_h(s-t)\left[\alpha(t) + \alpha'(t)(s-t) + \right. \\ \left. + \frac{\alpha''(t)}{2}(s-t)^2\right] Y(s)ds - \alpha'(t) + o_P\left(h^2\right). \end{aligned} \tag{A.1}$$

Expanding the brackets in the integrand and using the definition of moments a_j, for $j = 0, 1, 2, 3$, given in (A.6), it yields

$$B(t) = \frac{a_0(t)}{a_2(t)a_0(t) - a_1^2(t)}\left(\alpha(t)a_1(t) + \alpha'(t)a_2(t) + \frac{\alpha''(t)}{2}a_3(t)\right) \tag{A.2}$$

$$- \frac{a_1(t)}{a_2(t)a_0(t) - a_1^2(t)}\left(\alpha(t)a_0(t) + \alpha'(t)a_1(t) + \frac{\alpha''(t)}{2}a_2(t)\right) \tag{A.3}$$

$$- \alpha'(t) + o_P\left(h^2\right), \tag{A.4}$$

which can be reduced to the following expression

$$B(t) = \frac{a_3(t)a_0(t) - a_2(t)a_1(t)}{a_2(t)a_0(t) - a_1^2(t)} \frac{\alpha''(t)}{2} + o_P\left(h^2\right). \tag{A.5}$$

Using the continuity of the limiting function γ, the moments can be approximated by

$$a_j(t) = nh^j \gamma(t)\mu_j(K) + o_P\left(h^j\right), \tag{A.6}$$

for $j = 0, 1, \ldots$. Assumption $A2$ implies that the moments $\mu_j(K) = 0$, for $j = 1, 3$, whereas $\mu_0 = 1$, $\mu_2(K) > 0$. Finally using $A1$ it can be deduced the first term on the right side of (A.5) is also of order $o_P(h^2)$, then it is true that

$$B(t) = o_P\left(h^2\right). \tag{A.7}$$

As for the variance we consider the approximation of the moments $(A.6)$ in the integrand of $V(t)$ and define

$$V^*(t) = \int_0^T \frac{(s-t)}{nh^2\mu_2(K)\gamma(t)} K_h(s-t)dM(s) \tag{A.8}$$

and it can be seen that $\sup_{t\in[0,T]} |V^*(t) - V(t)| = o_P(1)$. Note that the integrand in $V^*(t)$ is predictable so we can use Proposition Appendix A. Define the following predictable process

$$W_{n,t}(s) = \left(nh^3\right)^{1/2} \frac{(s-t)}{nh^2\mu_2(K)\gamma(t)} K_h(s-t), \tag{A.9}$$

then it can be shown through the usual change of variable in the integral and using $A1 - A4$ that $\int_0^T W_{n,t}(s)^2 \alpha(s) Y(s) ds$ converges to the following limit

$$\sigma_t^2 = \frac{\alpha(t) \int u^2 K^2(u) du}{\gamma(t)\mu_2^2(K)} \tag{A.10}$$

The second part of the theorem is fulfilled given that $nh^3 \to +\infty$, and then we have that

$$\int W_{n,t}(s)dM(s) = \left(nh^3\right)^{1/2} V^*(t) \xrightarrow{D} N\left(0, \sigma_t^2\right), \tag{A.11}$$

which concludes the proof.

Remark: In survival analysis the interest is to model the lifetime of a subject. When the life process is represented by a counting process N under the Aalen's model, the process Y usually represents the at-risk process and is defined as taking value 1 when the subject is alive and under observation and 0 otherwise. In such cases, the function γ is the limiting exposure which is defined as $\gamma(t) = Pr\{Y(t) = 1\}$.